SUPPORTING METHODS

Model compartmentalization

The model was partitioned into separate intracellular and extracellular (growth media) compartments to enable experimental parameterization and validation (1). The governing system of differential mass balances,

$$\frac{d\boldsymbol{C}}{dt} = \hat{\boldsymbol{S}} \cdot \boldsymbol{r}_{\mathrm{I}} \tag{1}$$

is on a concentration (mol·vol^{-1}) basis, where $\boldsymbol{C}$ represents species concentrations (mol·vol^{-1}), $\boldsymbol{r}_{\mathrm{I}}$ is a vector of intensive reaction rates (mol·vol^{-1}·time^{-1}), and $\hat{\boldsymbol{S}}$ is the reaction stoichiometry matrix. Given that concentration is not conserved across regions of unequal volume (*e.g.*, between extracellular and intracellular compartments), entries in the $\hat{\boldsymbol{S}}$ matrix were scaled depending on species locations to uphold mass conservation. To represent the scaling explicitly, the balance was first rewritten on a mole basis:

$$\frac{d\boldsymbol{N}}{dt} = \boldsymbol{S} \cdot \boldsymbol{r}_{\mathrm{E}} \tag{2}$$

where $\boldsymbol{r}_{\mathrm{E}}$ are the extensive reaction rates (mol·time^{-1}), $\boldsymbol{N}$ represents the number of moles of each species, and $\boldsymbol{S}$ is the unscaled stoichiometry matrix, all of which are now independent of volume or compartment location. Since reaction rates are generally reported and used in their intensive form (mol·vol^{-1}·time^{-1}), the expression was rewritten in terms of $\boldsymbol{r}_{\mathrm{I}}$:

$$\frac{d\boldsymbol{N}}{dt} = \boldsymbol{S} \cdot \boldsymbol{V}_{\mathrm{rxn}} \cdot \boldsymbol{r}_{\mathrm{I}} \tag{3}$$

where $\boldsymbol{V}_{\mathrm{rxn}}$ is a diagonal matrix with entries corresponding to the volume of the compartment in which the reaction occurs (V_{cell} for intracellular reactions, V_{media} for extracellular reactions, and V_{total} for exchange reactions that span the two compartments). Furthermore, because experimental measurements were of species concentrations (*e.g.*, [NO•] and [O_2]) and not moles, both sides of the equation were divided by a volume term, $\boldsymbol{V}_{\mathrm{spec}}$:

$$\boldsymbol{V}_{\mathrm{spec}}^{-1} \cdot \frac{d\boldsymbol{N}}{dt} = \boldsymbol{V}_{\mathrm{spec}}^{-1} \cdot \boldsymbol{S} \cdot \boldsymbol{V}_{\mathrm{rxn}} \cdot \boldsymbol{r}_{\mathrm{I}} \tag{4}$$

where $\boldsymbol{V}_{\mathrm{spec}}$ is a diagonal matrix with entries corresponding to the volume of the compartment in which each species exists (V_{cell} for intracellular species, V_{media} for extracellular species, and V_{total} for species that rapidly diffuse across the membrane and exist in both compartments with equal concentration, such as NO• and O_2). Moles divided by volume ($\boldsymbol{V}_{\mathrm{spec}}^{-1} \cdot \boldsymbol{N}$) is equivalent to concentration ($\boldsymbol{C}$), and thus the equation becomes:

$$\frac{d\boldsymbol{C}}{dt} = \boldsymbol{V}_{\mathrm{spec}}^{-1} \cdot \boldsymbol{S} \cdot \boldsymbol{V}_{\mathrm{rxn}} \cdot \boldsymbol{r}_{\mathrm{I}} \tag{5}$$

In this form, the right-hand side of the balance is dependent on the absolute volumes of the media and cell compartments (V_{media} and V_{cell}), which is undesirable. Instead, the volume terms ($\boldsymbol{V}_{spec}$ and $\boldsymbol{V}_{rxn}$) can be scaled by V_{total} such that they are in terms of volume fractions (V_{cell}/V_{total} and V_{media}/V_{total}), which are easily estimated from the cell density (OD_{600}) of the culture. To perform the scaling, the right-hand side of the equation was multiplied by V_{total}/V_{total},

$$\frac{d\boldsymbol{C}}{dt} = \frac{V_{total}}{V_{total}} \boldsymbol{V}_{spec}^{-1} \cdot \boldsymbol{S} \cdot \boldsymbol{V}_{rxn} \cdot \boldsymbol{r}_{I} \tag{6}$$

and rearranged, using the commutative property of scalar multiplication:

$$\frac{d\boldsymbol{C}}{dt} = V_{total} \boldsymbol{V}_{spec}^{-1} \cdot \boldsymbol{S} \cdot \frac{\boldsymbol{V}_{rxn}}{V_{total}} \cdot \boldsymbol{r}_{I} \tag{7}$$

The V_{total} scalars were multiplied with $\boldsymbol{V}_{spec}$ and $\boldsymbol{V}_{rxn}$ such that the balance could be written in terms of volume fractions ($\boldsymbol{F}_{spec}$ and $\boldsymbol{F}_{rxn}$, respectively),

$$\frac{d\boldsymbol{C}}{dt} = \boldsymbol{F}_{spec}^{-1} \cdot \boldsymbol{S} \cdot \boldsymbol{F}_{rxn} \cdot \boldsymbol{r}_{I} \tag{8}$$

where:

$$\boldsymbol{F}_{spec} = \frac{\boldsymbol{V}_{spec}}{V_{total}}, \qquad \boldsymbol{F}_{rxn} = \frac{\boldsymbol{V}_{rxn}}{V_{total}}, \qquad \text{and } \hat{\boldsymbol{S}} = \boldsymbol{F}_{spec}^{-1} \cdot \boldsymbol{S} \cdot \boldsymbol{F}_{rxn} \tag{9}$$

Using this form of the balance (Equation 8), concentrations and reaction rates could be expressed in terms of the relevant compartment volume, without embedding the associated volume fraction into the stoichiometric coefficient matrix.

MCMC exploration of viable parameter space

An out-of-equilibrium adaptive Metropolis Markov chain Monte Carlo (MCMC) method (2) was employed to identify additional parameter sets exhibiting similar or improved quality of fit (quantified by AIC) compared to the parameter set obtained from the *lsqcurvefit* least-squares optimization. The MCMC method was run in MATLAB using the *MCexp* function from the HYPERSPACE software package (2), with a parameter evaluation limit of 10,000 and a cost function defined as the SSR between simulated and measured concentrations (SSR was scaled by experimental variance if no oscillations were present in the measured [NO•] curves). In the event that the MCMC method yielded more optimal (lower SSR) parameter sets such that the initial set exhibited an ER > 10 relative to the new minimum, the MCMC method was repeated, using the new minimum as the initial parameter set.

Training extracellular parameters

Extracellular model parameters were trained on measurements performed in the bioreactor in the absence of cells. The O_2 volumetric mass transfer coefficient ($k_L a_{O2}$) was measured by monitoring [O_2] in cell-free media after depleting the O_2 with an N_2 flush, as

described previously (3). A line was fit to the $ln([O_2]_{sat} - [O_2])$ vs. time data points, yielding a $k_L a_{O2}$ of 1.25×10^{-3} s^{-1}. The remaining extracellular parameters were determined through an optimization with [NO•] measurements in cell-free media. Parameters governing NO• autoxidation ($k_{NO•\text{-}O2}$), NO• loss to the gas phase ($k_L a_{NO•}$), and the rate of NO• dissociation from DPTA NONOate ($k_{NONOate,DPTA}$) were released to simultaneously fit [NO•] measured in cell-free MOPS media at 0 and 50 μM O_2 following treatment with 50 μM DPTA NONOate. Optimal values were $k_{NO•\text{-}O2} = 2.40 \times 10^6$ $M^{-2}s^{-1}$, $k_L a_{NO•} = 1.35 \times 10^{-3}$ s^{-1}, and $k_{NONOate,DPTA} = 7.73 \times 10^{-5}$ s^{-1}, and yielded [NO•] profiles in excellent agreement with experimental data (SI Appendix, Fig. S14*A*). Measurements of pH in *E. coli* cultures at 0 μM O_2 revealed that the media was slightly acidified (from 7.4 to 7.2), which was likely the result of mixed-acid fermentation. Therefore, the cell-free NO• measurement was repeated at 0 μM O_2 using pH-adjusted (w/ HCl) cell-free media (pH = 7.2), to replicate the conditions observed in the presence of cells. The value of $k_{NONOate,DPTA}$ was released (while fixing $k_{NO•\text{-}O2}$ and $k_L a_{NO•}$) to determine the DPTA NONOate release rate under anaerobic conditions. The optimal fit yielded a small increase in $k_{NONOate,DPTA}$ to 8.81×10^{-5} s^{-1}, and exhibited excellent agreement with measured [NO•] curve (SI Appendix, Fig. S14*A*).

Training the respiratory module

Uncertain model parameters involved in the aerobic respiratory chain were optimized to fit the simulated [O_2] curve to experimental measurements in a culture of exponential-phase *E. coli* grown in an environment of 50 μM O_2 (SI Appendix, Fig. S14*B* and Table S6). These 10 parameters were previously trained on [O_2] curves (4), but because those measurements were under fully-aerobic (210 μM O_2) conditions, and involved a centrifugation step immediately prior to inoculation of the cells, they were optimized for the present conditions. A subsequent individual parametric analysis was conducted to determine those parameters that were informed by the optimization, defined as those imparting a >5% increase in SSR when individually varied within their allowed bounds. All 10 parameters were identified as informed by the optimization, and the simulated [O_2] curve using the optimal parameter set was in excellent agreement with measurements under 50 μM and 10 μM O_2 conditions (SI Appendix, Fig. S14*B*).

Training cellular parameters on [NO•] measurements

For each optimization described below, the associated parameter bounds, optimal values, and confidence intervals can be found in Dataset S3, while the corresponding AIC and SSR of each best-fit parameter set are presented in SI Appendix, Table S2.

Initial optimization

Uncertain cellular parameters not associated with the respiratory module were released and optimized to fit [NO•] curves measured at 0 and 50 μM O_2. Using the best-fit model from the optimization, a parametric sensitivity analysis was conducted, and determined that 17 of the 50 released parameters were informed by the optimization. The MCMC method was used to further explore the viable parameter space defined by these 17 informed parameters, and yielded an additional 381 viable parameter sets with an ER < 10.

Optimization of model on all [O_2] conditions ("Stage 1")

The 17 parameters identified as important in the initial optimization were re-optimized to simultaneously fit [NO•] curves measured under conditions of 0, 5, 10, 20, and 50 μM O_2. The

optimized [NO•] curves exhibited improved agreement with measurements at 5, 10, and 20 μM O_2 relative to the original optimization, but at the expense of performance at 50 μM O_2. Given the poor performance of the model at 50 μM O_2, an MCMC analysis of the parameter space was not performed.

Release of all cellular parameters ("Stage 2")

To determine if the model could fit the measured [NO•] profiles under all [O_2] conditions explored (0, 5, 10, 20, and 50 μM O_2) without requiring a change to the network structure, all cellular parameters (136 kinetic rate constants and species concentrations specific to the organism) were released and optimized. Despite the increased parametric flexibility, the optimization did not yield a lower AIC, as the reduction in SSR was insufficient to offset the penalty of including additional parameters. As such, an MCMC analysis was not performed.

Optimization of model with [O_2]-dependent translation ("Stage 3")

After implementing an [O_2] dependency in the rate of translation, the 17 parameters from the initial optimization, as well as the two new parameters introduced with the new translation rate equation ($k_{act,O2}$ and $K_{d,O2}$), were optimized on the [NO•] curves measured at the five different O_2 concentrations. The optimization yielded a parameter set with a sufficient decrease in SSR to justify the inclusion of the two additional parameters, as quantified by a decrease in AIC. An MCMC walk from the optimal parameter set yielded an additional 2,339 viable parameter sets with an ER < 10.

Inclusion of CYT-related parameters in model optimization ("Stage 4")

After performing the reaction deletion analysis, which predicted the involvement of CYT in [NO•] oscillations, four parameters governing the NO•-mediated inhibition of CYT ($k_{CYTbo,NO•-on}$, $k_{CYTbd,NO•-on}$, $K_{m,CYTbo,O2}$, and $K_{m,CYTbd,O2}$) were released for optimization on [NO•] curves at all measured [O_2] conditions, along with the 19 parameters included in the previous optimization. The best-fit model obtained from the optimization exhibited sufficient improvement in SSR to offset the penalty of releasing four additional parameters (AIC was decreased). A subsequent run of the MCMC method provided 240 additional viable parameter sets with an ER < 10.

Parameter optimization on CAM-treated [NO•] data

Treatment with CAM (a translation inhibitor) was accomplished *in silico* by simulating NO• treatment (at 10 μM O_2) for 1.5 h, setting all translation rates to zero, and resuming the simulation. The 23 parameters released in the previous optimization were again allowed to vary in an effort to fit the experimental CAM-treated [NO•] data. Simulated [NO•] curves with the optimal parameter set were in excellent agreement with measurements, and an MCMC walk generated an additional 668 viable parameter sets with ER < 10.

SUPPORTING FIGURES

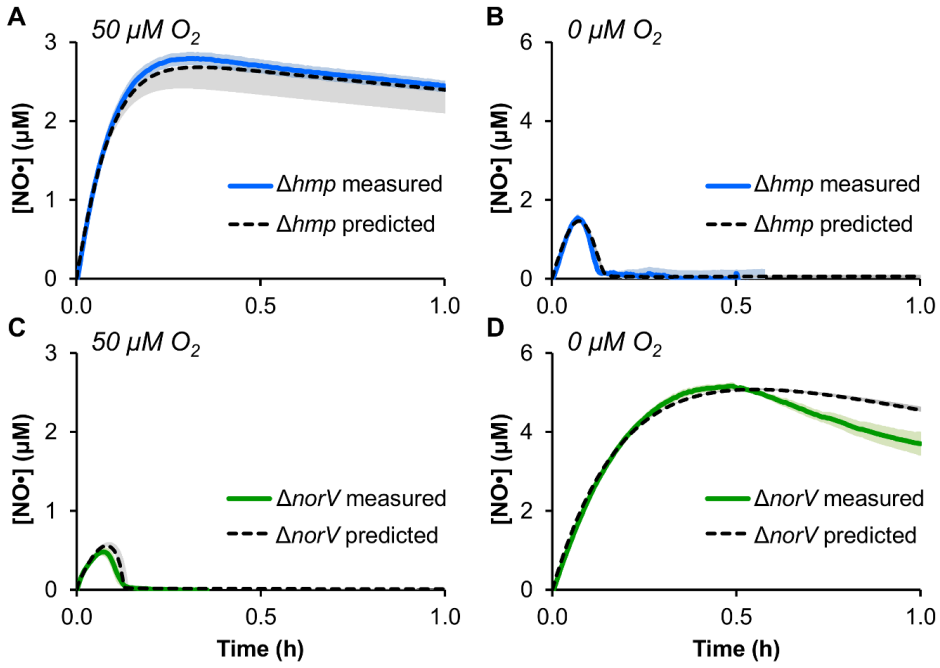

Fig. S1. Experimental validation of predicted Δ*hmp* and Δ*norV* [NO•] at 50 and 0 μM O_2. NO• treatment (50 μM DPTA NONOate) was simulated using parameter values trained on WT [NO•] measurements at 50 and 0 μM O_2 to predict the effect of the Δ*hmp* mutation on NO• clearance at (*A*) 50 μM O_2 and (*B*) 0 μM O_2, as well as (*C*) Δ*norV* at 50 μM O_2 and (*D*) 0 μM O_2. Black dashed lines are simulations using the best-fit (minimum SSR, ER = 1) parameter set, where gray shading represents prediction uncertainty (range of viable parameter sets with ER < 10). The corresponding experimental measurements were performed, wherein exponential-phase Δ*hmp* or Δ*norV E. coli* (OD_{600} = 0.05) were treated with 50 μM DPTA NONOate at 50 or 0 μM O_2 (solid lines; mean of three independent experiments with shading representing the SEM). The O_2 concentration corresponds to the concentration of dissolved O_2 in cell-free media that was in equilibrium with the atmosphere of the hypoxic chamber.

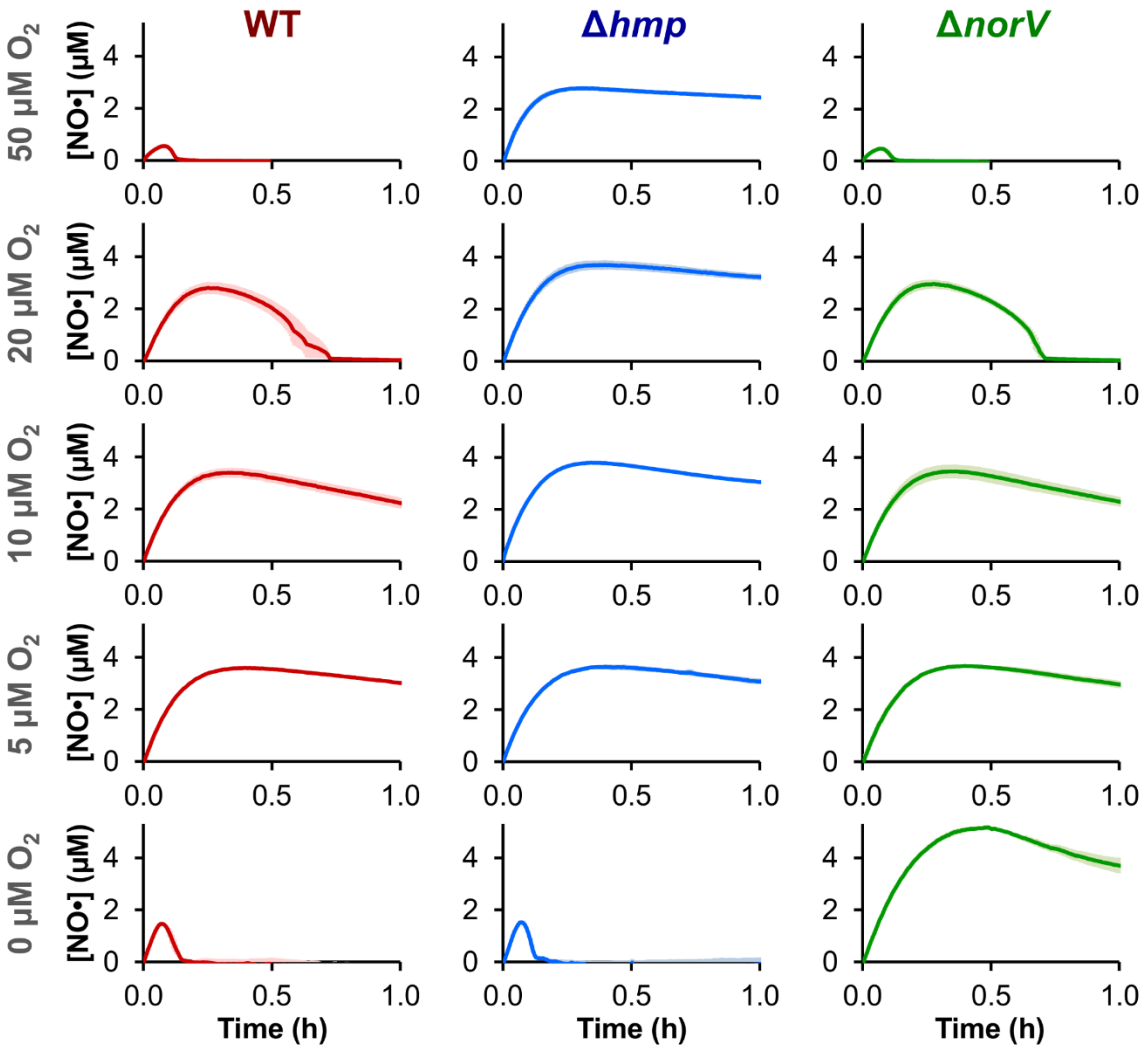

Fig. S2. NO• detoxification in WT, Δ*hmp*, and Δ*norV* cultures under various [O_2]. Cultures of WT, Δ*hmp*, or Δ*norV E. coli* (OD_{600} = 0.05) were treated with 50 μM DPTA NONOate at 50, 20, 10, 5, and 0 μM [O_2], and the resulting [NO•] was measured, showing up to 1 h post-dose. Data are the mean of at least 3 independent experiments, where shading of a similar color represents the SEM.

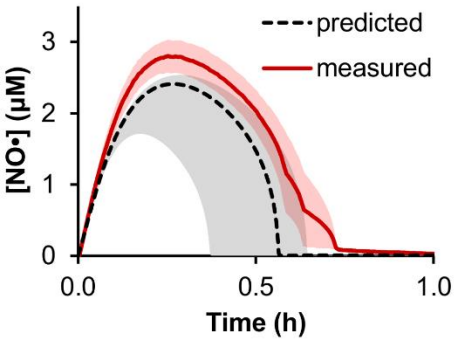

Fig. S3. Comparison of predicted and measured [NO•] at 20 μM O_2. Shown are the predicted (dashed black lines) and measured (solid red lines) [NO•] curves following treatment of WT *E. coli* (OD_{600} = 0.05) with 50 μM DPTA NONOate at 20 μM O_2. The measured [NO•] is the mean of 3 independent experiments, with light red shading representing the SEM. Predicted [NO•] curves were obtained using the best-fit parameter set (from initial optimization on [NO•] measured at 0 and 50 μM O_2), with gray shading representing prediction uncertainty (range of viable parameter sets with ER < 10).

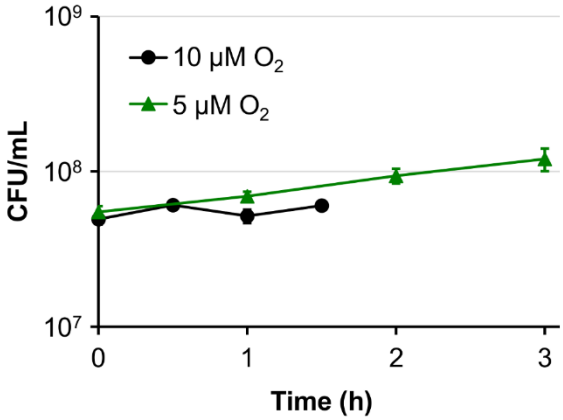

Fig. S4. Assessing cell culturability during NO• treatment at 5 and 10 μM O_2. WT *E. coli* at an OD_{600} of 0.05 were treated with 50 μM DPTA NONOate at 5 or 10 μM O_2. Samples were removed immediately prior to DPTA NONOate treatment, and at 3 additional time points post-treatment, and plated on LB + agar to determine the concentration of colony forming units (CFUs). Measurements were made out to 1.5 and 3 h post-dose for 10 and 5 μM O_2, respectively, as NO• was largely cleared from the culture by those times. Data are the mean of 3 independent experiments, with error bars representing the SEM.

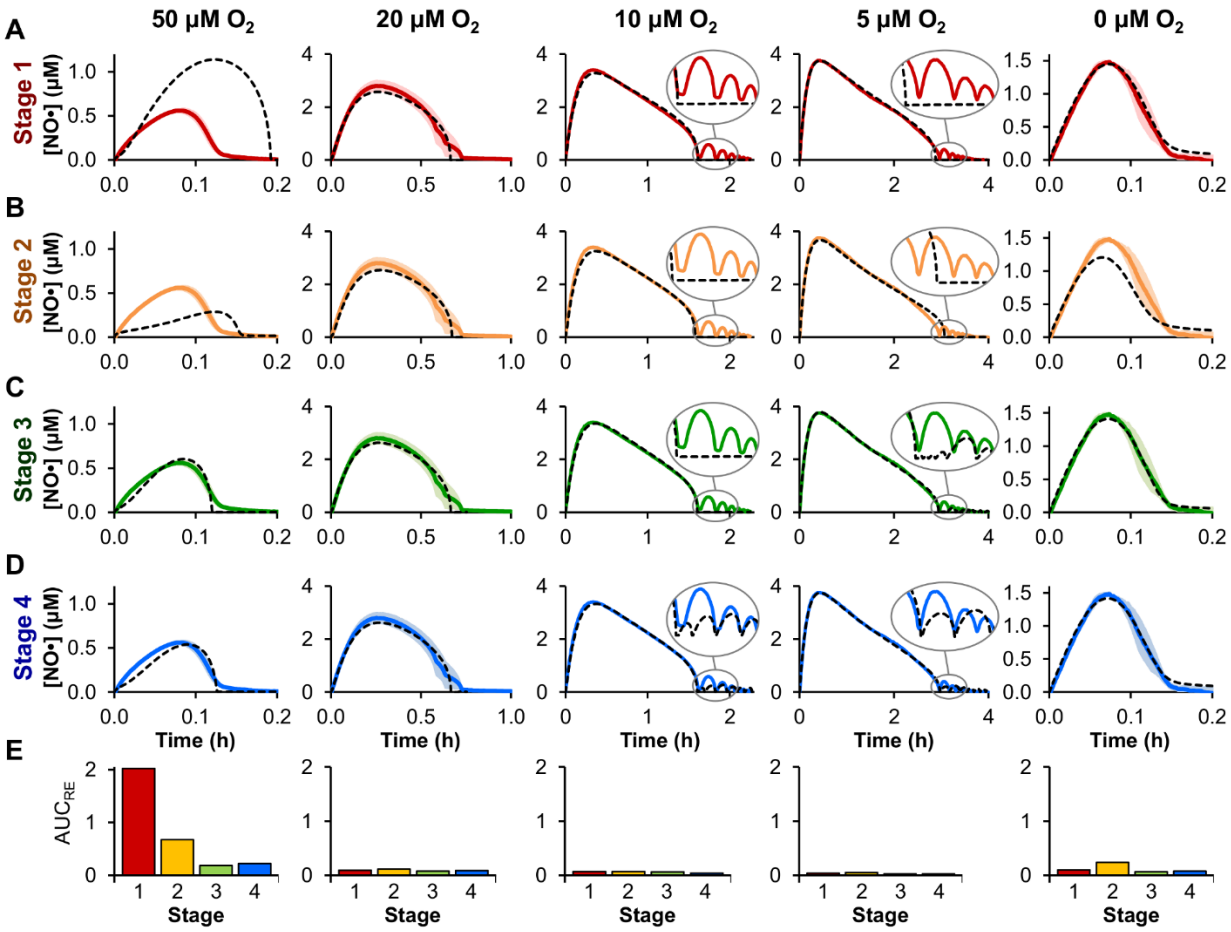

Fig. S5. Assessment of model performance at each stage of parameter optimization. Cultures of WT *E. coli* (OD_{600} = 0.05) were treated with 50 μM DPTA NONOate at 50, 20, 10, 5, and 0 μM O_2 and the resulting [NO•] was measured (solid lines). Measured [NO•] curves without oscillations (0, 20, and 50 μM O_2) are the mean of at least 3 independent experiments with shading representing the SEM, while those with oscillations (5 and 10 μM O_2) are a representative measurement of at least 3 independent experiments (the results of which are shown in SI Appendix, Figs. S13 *A* and *C*). Model parameters were trained on measured [NO•] from all five O_2 conditions, where the simulation run using the best-fit parameter set is shown (black dashed lines). For 5 and 10 μM O_2 conditions, a region of the [NO•] plot is magnified to more easily view oscillations. (*A*) *Stage 1*: 17 parameters were optimized, using the original model structure (without O_2-dependent translation rate). (*B*) *Stage 2*: all 136 cellular parameters were optimized, using the original model structure. (*C*) *Stage 3*: 19 parameters were optimized, where the 2 additional parameters ($k_{act,O2}$ and $K_{d,O2}$) were those governing the added O_2-dependency of the translation rate. (*D*) *Stage 4*: 23 parameters were optimized, where the 4 additional parameters ($k_{CYTbo,NO•\text{-}on}$, $k_{CYTbd,NO•\text{-}on}$, $K_{m,CYTbo,O2}$, and $K_{m,CYTbd,O2}$) were those governing kinetics of NO•-mediated cytochrome inhibition (again using the O_2-dependent translation rate equation). (*E*) Comparison of AUC_{RE} (relative area-under-the-curve error) calculated for simulated vs. measured [NO•] for each optimization stage (red, yellow, green, and blue bars for *Stages 1–4*, respectively).

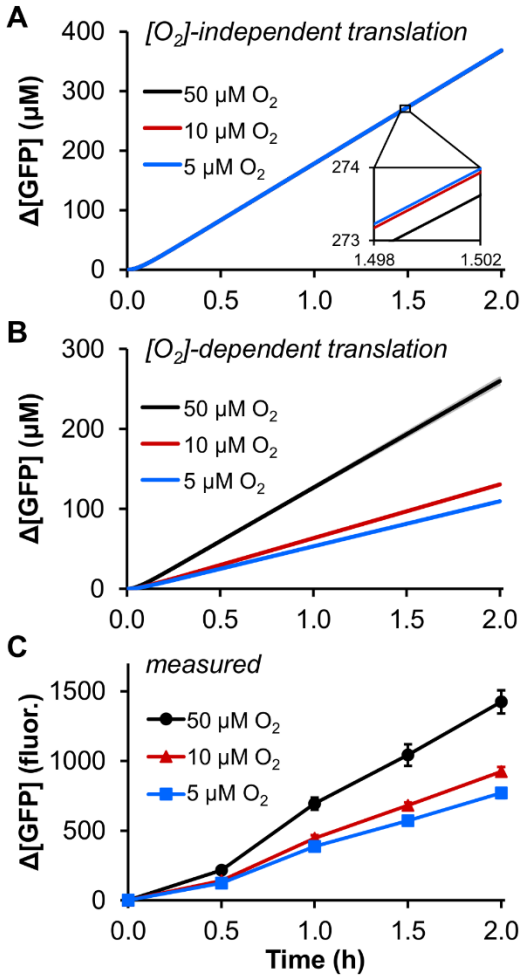

Fig. S6. Experimental confirmation of the predicted effect of [O_2] on translation. Production of GFP (driven by the P_{hmp} promoter in Δ*hmp E. coli*; see *Methods*) following treatment with 50 μM DPTA NONOate at 5, 10, and 50 μM O_2 was predicted using (*A*) the original model structure, which excluded an [O_2]-dependent translation rate, and (*B*) the revised model structure, which included an [O_2]-dependent translation rate (optimization "Stage 1" and "Stage 3", respectively). Predicted curves were generated using the best-fit parameter set, with shading representing prediction uncertainty (range of viable parameter sets with ER < 10). The inset in (*A*) is provided to demonstrate that all three curves are present, but nearly aligned. (*C*) The corresponding experiments were performed, where Δ*hmp E. coli* possessing P_{hmp}-GFP on a plasmid were treated with 50 μM DPTA NONOate (OD_{600} = 0.05), and samples were removed every 30 min to quantify GFP fluorescence (485 nm excitation, 515 nm emission). Fluorescence measured at the time of treatment (t = 0) was subtracted from each reading to determine the change in protein abundance (Δ[GFP]). Fluorescence data are the mean of 3 independent experiments, with error bars representing the SEM.

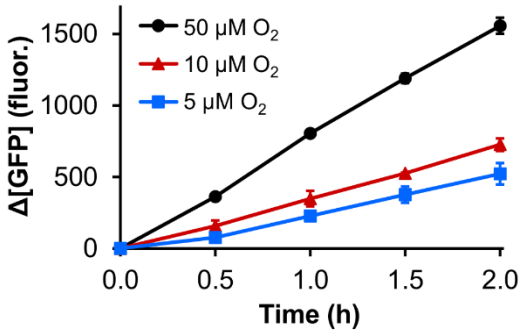

Fig. S7. Assessing whether the effect of [O_2] on translation is specific to P_{hmp} and NO• stress conditions. WT *E. coli* possessing an IPTG-inducible P_{T5}-GFP on a plasmid were grown to exponential phase, delivered to the bioreactor to an initial OD_{600} of 0.05, and induced immediately with 1 mM IPTG (in the absence of NO•). Samples were taken every 30 min and diluted to maintain a constant OD_{600} of 0.05 prior to fluorescence quantification, as cells were growing due to the lack of NO• treatment. The assay was conducted at 5, 10, and 50 μM O_2. Data are the mean of 3 independent experiments, with error bars representing the SEM.

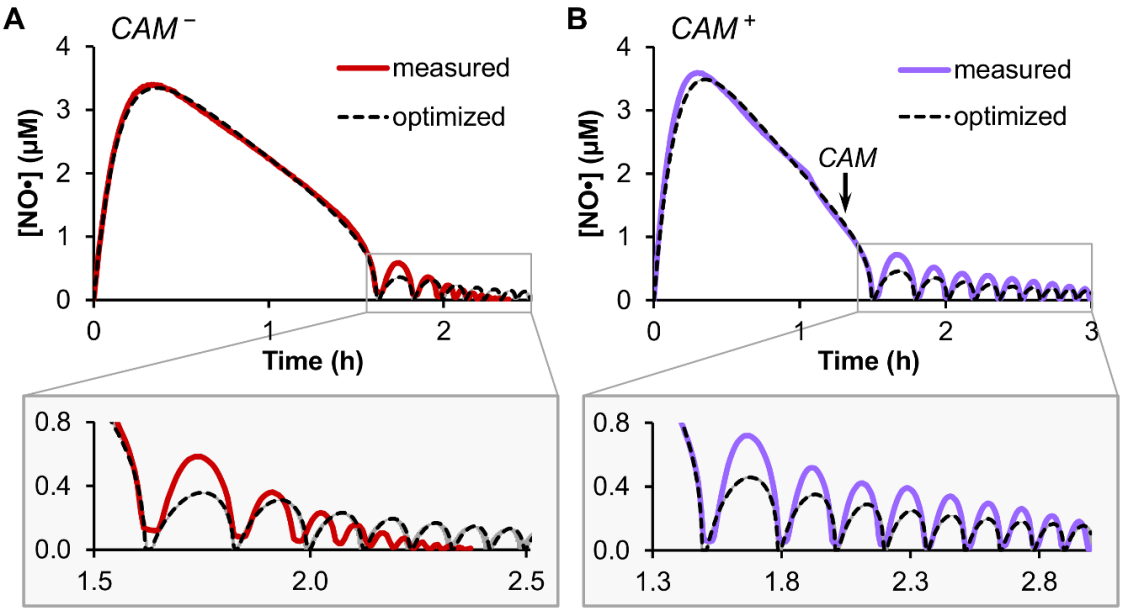

Fig. S8. [NO•] oscillation dynamics in the presence and absence of translation. [NO•] was measured in cultures of WT *E. coli* following treatment with 50 μM DPTA NONOate at 10 μM O_2, either (*A*) without or (*B*) with 100 μg/mL CAM treatment at t = 1.25 h (~15 min prior to initial NO• clearance, indicated by arrow). Measured [NO•] (solid lines) are representative of at least 3 independent experiments, the results of which are shown in SI Appendix, Figs. S13 *A* and *G* (for CAM^- and CAM^+, respectively). Simulated [NO•] curves (dashed black lines) represent the best-fit parameter set obtained from an optimization on the measured WT [NO•] curve at 10 μM O_2 (*A*) without or (*B*) with CAM, where CAM treatment was simulated by fixing the translation rate to zero at the time of initial NO• clearance. Gray shading on the optimized [NO•] curves (very small) represent the range of simulations from viable parameter sets with ER < 10.

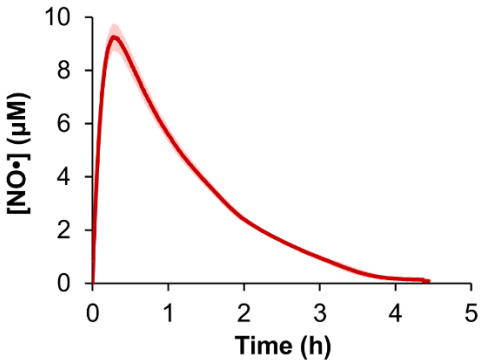

Fig. S9. NO• detoxification in WT *P. aeruginosa* cultures at 10 μM O_2. *P. aeruginosa* in BSM + 15 mM succinate media at an OD_{600} of 0.05 was treated with 50 μM DPTA NONOate in an environment of 10 μM O_2, and the resulting concentration of NO• was measured. The data are the mean of 3 independent experiments, with light red shading representing the SEM.

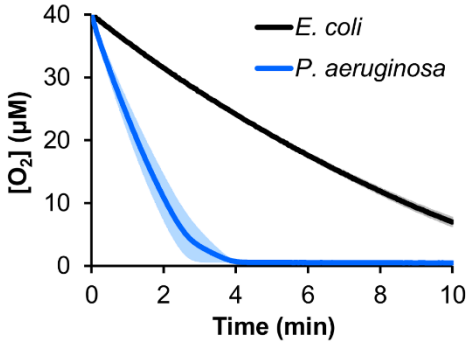

Fig. S10. Comparison of *E. coli* and *P. aeruginosa* O_2 consumption rate. WT *E. coli* or *P. aeruginosa* were grown to mid-exponential phase in an environment of 50 μM O_2 and diluted into the bioreactor (OD_{600} = 0.05), and the resulting [O_2] was measured. Time zero was set as the time at which [O_2] = 40 μM, to facilitate direct comparison between the [O_2] curves. Data are the mean of 3 independent experiments, with shading representing the SEM.

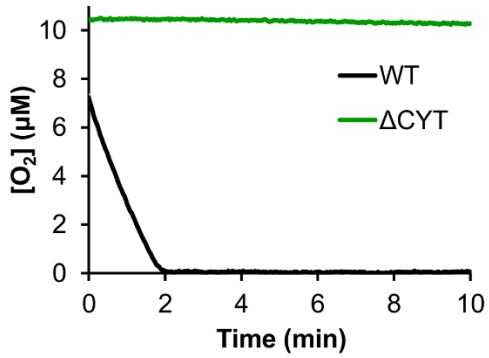

Fig. S11. Experimental confirmation of negligible O_2 consumption by ΔCYT. Cultures of WT or ΔCYT *E. coli* were grown under a 10 μM O_2 environment to exponential phase, diluted to an OD_{600} of 0.05 in the bioreactor, and [O_2] was monitored. The WT culture began at a moderately lower [O_2] (~7 μM) due to O_2-depletion in the inoculum (caused by cellular respiration in a more concentrated culture). Data are the average of 3 independent experiments, with shading (very small) representing the SEM.

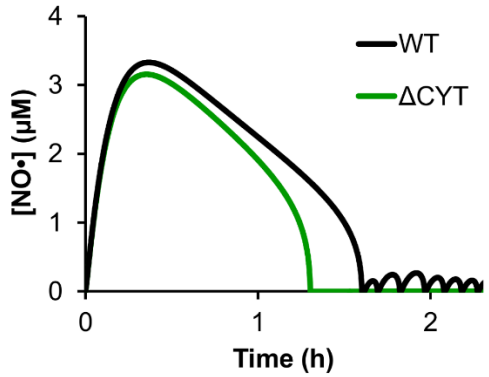

Fig. S12. Predicted elimination of oscillations upon CYT deletion. Simulated [NO•] resulting from the treatment of WT or ΔCYT cultures with 50 μM DPTA NONOate, using parameters values obtained from optimization "Stage 4." Solid lines are the best-fit parameter set, with shading (very small) representing prediction uncertainty. Predictions assumed the typical pH of 7.4 exhibited by WT cultures grown in the presence of O_2.

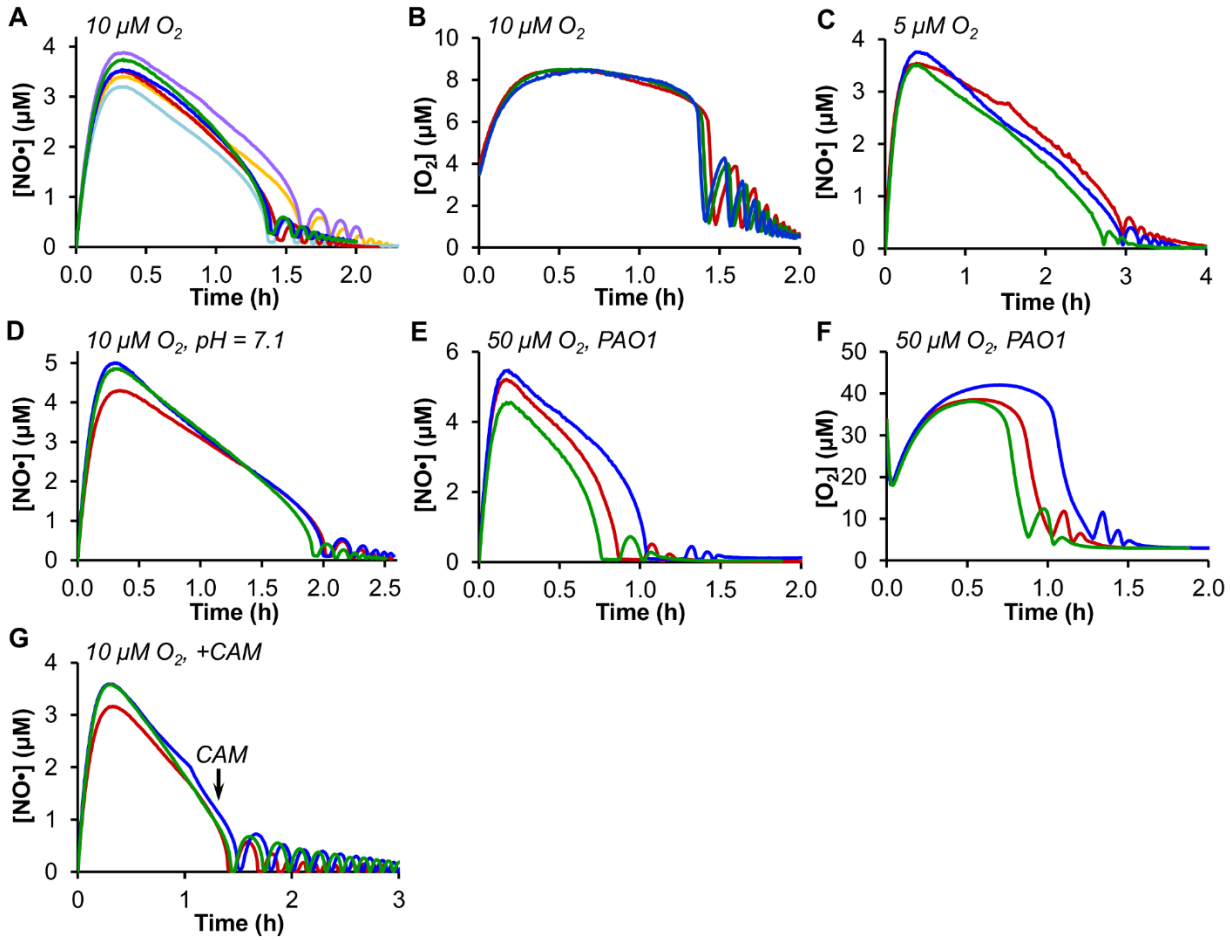

Fig. S13. Experimental replicates for [NO•] and [O_2] curves exhibiting oscillations. Given that small shifts in NO• clearance time or oscillation phase yield average [NO•] or [O_2] curves that obscured the dynamics of the oscillations, figures in the present study typically show a representative experiment (rather than the average of all replicates) for concentration curves exhibiting oscillations. For completeness, all experimental replicates are presented here for any condition for which a representative curve was presented in another figure. (*A*) [NO•] and (*B*) [O_2] was measured in cultures of WT *E. coli* (OD_{600} = 0.05) treated with 50 μM DPTA NONOate at 10 μM O_2, or (*C*) [NO•] was measured at 5 μM O_2. (*D*) Identical conditions as (*A*), except the pH was adjusted to 7.1 (from 7.4) immediately prior to DPTA NONOate treatment. (*E*) [NO•] and (*F*) [O_2] were measured in cultures of *P. aeruginosa* treated with 50 μM DPTA NONOate at 50 μM O_2 and 0.05 OD_{600} in BSM + succinate media. (*G*) Identical to (*A*), except cultures were treated with 100 μg/mL CAM ~15 min prior to the initial NO• clearance time (1.25 h after DPTA NONOate treatment). Each colored curve represents an independent experimental replicate.

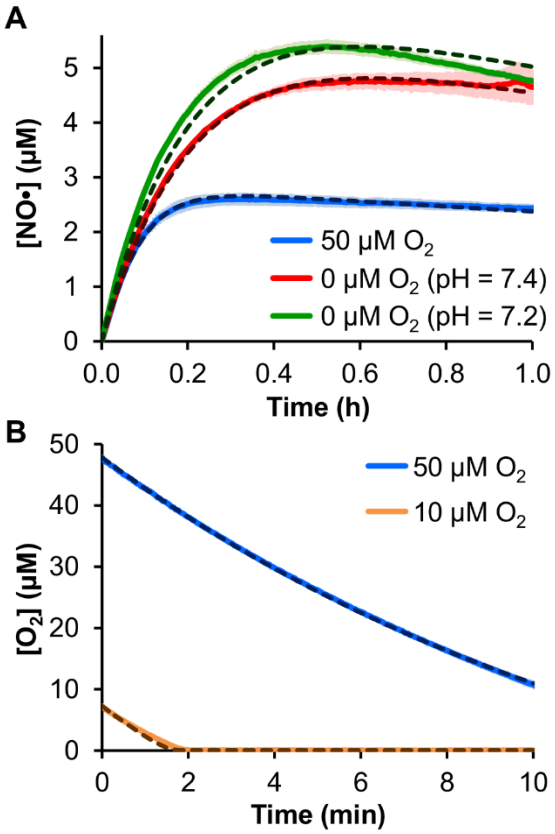

Fig. S14. Training of extracellular parameters and the respiratory module. (*A*) Cell-free media (MOPS minimal media with 10 mM glucose) was treated with 50 μM DPTA NONOate at 0 and 50 μM O_2, and the resulting [NO•] was measured (solid red and blue lines, respectively). Extracellular model parameters ($k_{NO•\text{-}O2}$, $k_La_{NO•}$, and $k_{NONOate,DPTA}$) were optimized on the two measured curves, yielding the simulated [NO•] shown (dashed dark red and dashed dark blue lines for 0 and 50 μM O_2, respectively). Since a pH decrease was observed in anaerobic WT *E. coli* cultures (decreased pH from 7.4 to 7.2 upon bioreactor inoculation to OD_{600} = 0.05 prior to NO• treatment), which increases the rate of DPTA NONOate dissociation ($k_{NONOate,DPTA}$), the [NO•] measurement at 0 μM O_2 was repeated in cell-free media that had been adjusted to a pH of 7.2 with HCl (solid green line). The $k_{NONOate,DPTA}$ parameter was released and trained on the pH-adjusted anaerobic [NO•] data (maintaining the same $k_{NO•\text{-}O2}$ and $k_La_{NO•}$ values obtained from the original optimization), yielding the simulated [NO•] curve shown (dashed dark green line). Experimental data are the mean of 3 independent experiments, with shading representing the SEM. (*B*) WT *E. coli* was grown to exponential phase in an environment of 50 μM O_2 and diluted into the bioreactor (OD_{600} = 0.05) at time t = 0, and the resulting [O_2] was measured (solid blue line). Model parameters associated with aerobic respiration were trained on the measured [O_2] curve (see *Methods* and SI Appendix, Table S6), and the resulting simulated [O_2] is shown (dashed dark blue line). The optimized parameter set was used to predict the [O_2] curve for a 10 μM O_2 environment (dashed brown line), and was in excellent agreement with the corresponding experimental measurement (solid orange line). Experimental data are the mean of 3 independent experiments, with shading representing the SEM.

SUPPORTING TABLES

Table S1. Model reactions governed by non-elementary type rate expressions. Reaction names, rate expressions, and rate constants are shown. The numbering of reactions is continued from Dataset S2. An asterisk "*" indicates kinetic parameters whose values were trained on experimental measurements in the present study. All reactions presented here occur within the intracellular compartment, unless otherwise noted.

#	Reaction name, equation, and kinetic expression		Parameters	Refs. [a]
161	"ISCUloadS1"	$\mathrm{IscU + 2\ Cys \xrightarrow{IscS} IscU(2S)^{2-} + 2\ Ala + 2\ H^+}$	k_{cat} = 0.07 s^{-1} K_{Cys} = (1–100)×10^{-6} M * K_{IscU} = (1–100)×10^{-6} M *	(5) (5) (5,6)
		$r = \frac{k_{cat}[\mathrm{IscS}][\mathrm{IscU}][\mathrm{Cys}]}{[\mathrm{IscU}][\mathrm{Cys}] + K_{Cys}[\mathrm{IscU}] + K_{IscU}[\mathrm{Cys}]}$		
162	"ISCUloadS2"	$\mathrm{IscU([2Fe\text{-}2S])^{2-} + 2\ Cys \xrightarrow{IscS} IscU([2Fe\text{-}2S]\text{-}2S)^{4-} + 2\ Ala + 2\ H^+}$	k_{cat} = 0.07 s^{-1} K_{Cys} = (1–100)×10^{-6} M * K_{IscU} = (1–100)×10^{-6} M *	(5) (5) (5,6)
		$r = \frac{k_{cat}[\mathrm{IscS}][\mathrm{IscU(2Fe2S)}][\mathrm{Cys}]}{[\mathrm{IscU(2Fe2S)}][\mathrm{Cys}] + K_{Cys}[\mathrm{IscU(2Fe2S)}] + K_{IscU(2Fe2S)}[\mathrm{Cys}]}$		
163	"isc2Fe2Srep1"	$P_{2Fe2S}(apo) + \mathrm{IscU([2Fe\text{-}2S])^{2-} + ATP + H_2O \xrightarrow{HscAB} IscU} + P_{2Fe2S}(holo) + \mathrm{ADP + P_i + H^+}$	k_{cat} = (1–1000)×10^{-4} s^{-1} * $K_{P2Fe2S(apo)}$ = (1–100)×10^{-6} M *	(7) (7)
		$r = \frac{k_{cat}[\mathrm{IscU(2Fe2S)}][P_{2Fe2S}(apo)]}{K_{P_{2Fe2S}(apo)} + [P_{2Fe2S}(apo)]}$		
164	"isc2Fe2Srep2"	$P_{2Fe2S}(apo) + \mathrm{IscU([2Fe\text{-}2S]_2)^{4-} + ATP + H_2O \xrightarrow{HscAB} IscU([2Fe\text{-}2S]) + } P_{2Fe2S}(holo) + \mathrm{ADP + P_i + H^+}$	k_{cat} = (1–1000)×10^{-4} s^{-1} * $K_{P2Fe2S(apo)}$ = (1–100)×10^{-6} M *	(7) (7)
		$r = \frac{k_{cat}[\mathrm{IscU(2Fe2S)_2}][P_{2Fe2S}(apo)]}{K_{P_{2Fe2S}(apo)} + [P_{2Fe2S}(apo)]}$		
165	"dXTSNbe"	$\mathrm{DNA(dX) + H_2O \xrightarrow{AlkA} DNA(AP_G) + X}$	k_{cat} = 4.0×10^{-4} s^{-1} $K_{DNA(dX)}$ = (1–100)×10^{-8} M *	(8) (8)
		$r = \frac{k_{cat}[\mathrm{AlkA}][\mathrm{DNA(dX)}]}{K_{DNA(dX)} + [\mathrm{DNA(dX)}]}$		
166	"dINbe"	$\mathrm{DNA(dI) + H_2O \xrightarrow{AlkA} DNA(AP_A) + hX}$	k_{cat} = 1.3×10^{-3} s^{-1} $K_{DNA(dI)}$ = (1–100)×10^{-8} M *	(9) (9)
		$r = \frac{k_{cat}[\mathrm{AlkA}][\mathrm{DNA(dI)}]}{K_{DNA(dI)} + [\mathrm{DNA(dI)}]}$		

167	"dURIbe"	$\mathrm{DNA(dU) + H_2O \xrightarrow{Ung} DNA(AP_C) + U}$	$k_{cat} = 0.5\ s^{-1}$ $K_{DNA(dU)} = (1–100)\times10^{-8}$ M *	(10) (10,11)
		$r = \frac{k_{cat}[\mathrm{Ung}][\mathrm{DNA(dU)}]}{K_{DNA(dU)} + [\mathrm{DNA(dU)}]}$		
168	"APgrem"	$\mathrm{DNA(AP_G) + 2\ H_2O \xrightarrow{Xth} DNA(dG)_{gap} + 2\ H^+ + dR5P}$	$k_{cat} = 0.23\ s^{-1}$ $K_{DNA(APG)} = 1.6\times10^{-8}$ M	(12) (12)
		$r = \frac{k_{cat}[\mathrm{Xth}][\mathrm{DNA(AP_G)}]}{K_{DNA(AP_G)} + [\mathrm{DNA(AP_G)}]}$		
169	"AParem"	$\mathrm{DNA(AP_A) + 2\ H_2O \xrightarrow{Xth} DNA(dA)_{gap} + 2\ H^+ + dR5P}$	$k_{cat} = 0.23\ s^{-1}$ $K_{DNA(APA)} = 1.6\times10^{-8}$ M	(12) (12)
		$r = \frac{k_{cat}[\mathrm{Xth}][\mathrm{DNA(AP_A)}]}{K_{DNA(AP_A)} + [\mathrm{DNA(AP_A)}]}$		
170	"APcrem"	$\mathrm{DNA(AP_C) + 2\ H_2O \xrightarrow{Xth} DNA(dC)_{gap} + 2\ H^+ + dR5P}$	$k_{cat} = 0.23\ s^{-1}$ $K_{DNA(APC)} = 1.6\times10^{-8}$ M	(12) (12)
		$r = \frac{k_{cat}[\mathrm{Xth}][\mathrm{DNA(AP_C)}]}{K_{DNA(AP_C)} + [\mathrm{DNA(AP_C)}]}$		
171	"dGSNpol"	$\mathrm{DNA(dG)_{gap} + dGTP \xrightarrow{PolI} DNA(dG)_{nick} + PP_i}$	$k_{cat} = 14\ s^{-1}$ $K_{DNA(dG)gap} = 5.4\times10^{-9}$ M $K_{i,DNA(dG)gap} = 8.1\times10^{-9}$ M $K_{i,DNA(dG)nick} = 2.2\times10^{-8}$ M $K_{dGTP} = 1.3\times10^{-6}$ M	(13) (13) (13) (13) (14)
		$r = \frac{k_{cat}[\mathrm{PolI}][\mathrm{dGTP}][\mathrm{DNA(dG)_{gap}}]}{K_{i,DNA(dG)_{gap}}K_{dGTP} + K_{DNA(dG)_{gap}}[\mathrm{dGTP}] + K_{dGTP}[\mathrm{DNA(dG)_{gap}}]\left(1+\frac{K_{i,DNA(dG)_{gap}}}{K_{i,DNA(dG)_{nick}}}\right) + [\mathrm{DNA(dG)_{gap}}][\mathrm{dGTP}]\left(1+\frac{K_{DNA(dG)_{gap}}}{K_{i,DNA(dG)_{nick}}}\right)}$		
172	"dDADpol"	$\mathrm{DNA(dA)_{gap} + dATP \xrightarrow{PolI} DNA(dA)_{nick} + PP_i}$	$k_{cat} = 14\ s^{-1}$ $K_{DNA(dA)gap} = 5.4\times10^{-9}$ M $K_{i,DNA(dA)gap} = 8.1\times10^{-9}$ M $K_{i,DNA(dA)nick} = 2.2\times10^{-8}$ M $K_{dATP} = 3.7\times10^{-6}$ M	(13) (13) (13) (13) (14)
		$r = \frac{k_{cat}[\mathrm{PolI}][\mathrm{dATP}][\mathrm{DNA(dA)_{gap}}]}{K_{i,DNA(dA)_{gap}}K_{dATP} + K_{DNA(dA)_{gap}}[\mathrm{dATP}] + K_{dATP}[\mathrm{DNA(dA)_{gap}}]\left(1+\frac{K_{i,DNA(dA)_{gap}}}{K_{i,DNA(dA)_{nick}}}\right) + [\mathrm{DNA(dA)_{gap}}][\mathrm{dATP}]\left(1+\frac{K_{DNA(dA)_{gap}}}{K_{i,DNA(dA)_{nick}}}\right)}$		

173	"dCYTpol"	$\mathrm{DNA(dC)_{gap} + dCTP \xrightarrow{PolI} DNA(dC)_{nick} + PP_i}$	$k_{cat} = 14\ s^{-1}$ $K_{DNA(dC)gap} = 5.4\times10^{-9}$ M $K_{i,DNA(dC)gap} = 8.1\times10^{-9}$ M $K_{i,DNA(dC)nick} = 2.2\times10^{-8}$ M $K_{dCTP} = 2.1\times10^{-6}$ M	(13) (13) (13) (13) (14)
		$r = \frac{k_{cat}[\mathrm{PolI}][\mathrm{dCTP}][\mathrm{DNA(dC)_{gap}}]}{K_{i,\mathrm{DNA(dC)_{gap}}}K_{dCTP} + K_{\mathrm{DNA(dC)_{gap}}}[\mathrm{dCTP}] + K_{dCTP}[\mathrm{DNA(dC)_{gap}}]\left(1+\frac{K_{i,\mathrm{DNA(dC)_{gap}}}}{K_{i,\mathrm{DNA(dC)_{nick}}}}\right) + [\mathrm{DNA(dC)_{gap}}][\mathrm{dCTP}]\left(1+\frac{K_{\mathrm{DNA(dC)_{gap}}}}{K_{i,\mathrm{DNA(dC)_{nick}}}}\right)}$		
174	"dGSNlig"	$\mathrm{DNA(dG)_{nick} + NAD^+ \xrightarrow{LigA} DNA(dG) + AMP + NMN + H^+}$	$k_{cat} = 0.023\ s^{-1}$ $K_{NAD+} = 7.0\times10^{-6}$ M $K_{DNA(dG)nick} = 5.0\times10^{-8}$ M	(15) (15) (15)
		$r = \frac{k_{cat}[\mathrm{LigA}][\mathrm{DNA(dG)_{nick}}][\mathrm{NAD^+}]}{[\mathrm{DNA(dG)_{nick}}][\mathrm{NAD^+}] + K_{\mathrm{NAD^+}}[\mathrm{DNA(dG)_{nick}}] + K_{\mathrm{DNA(dG)_{nick}}}[\mathrm{NAD^+}]}$		
175	"dDADlig"	$\mathrm{DNA(dA)_{nick} + NAD^+ \xrightarrow{LigA} DNA(dA) + AMP + NMN + H^+}$	$k_{cat} = 0.023\ s^{-1}$ $K_{NAD+} = 7.0\times10^{-6}$ M $K_{DNA(dA)nick} = 5.0\times10^{-8}$ M	(15) (15) (15)
		$r = \frac{k_{cat}[\mathrm{LigA}][\mathrm{DNA(dA)_{nick}}][\mathrm{NAD^+}]}{[\mathrm{DNA(dA)_{nick}}][\mathrm{NAD^+}] + K_{\mathrm{NAD^+}}[\mathrm{DNA(dA)_{nick}}] + K_{\mathrm{DNA(dA)_{nick}}}[\mathrm{NAD^+}]}$		
176	"dCYTlig"	$\mathrm{DNA(dC)_{nick} + NAD^+ \xrightarrow{LigA} DNA(dC) + AMP + NMN + H^+}$	$k_{cat} = 0.023\ s^{-1}$ $K_{NAD+} = 7.0\times10^{-6}$ M $K_{DNA(dC)nick} = 5.0\times10^{-8}$ M	(15) (15) (15)
		$r = \frac{k_{cat}[\mathrm{LigA}][\mathrm{DNA(dC)_{nick}}][\mathrm{NAD^+}]}{[\mathrm{DNA(dC)_{nick}}][\mathrm{NAD^+}] + K_{\mathrm{NAD^+}}[\mathrm{DNA(dC)_{nick}}] + K_{\mathrm{DNA(dC)_{nick}}}[\mathrm{NAD^+}]}$		
177	"GSFDH"	$\mathrm{GSNO + 2\ NADH + 2\ H^+ + GSH \xrightarrow{GSFDH} GSSG + NH_3 + H_2O + 2\ NAD^+}$	$k_{cat} = 3.1\times10^{-3}\ s^{-1}$ $K_{GSNO} = 7.4\times10^{-4}$ M	(16) (16)
		$r = \frac{k_{cat}[\mathrm{GSFDH}][\mathrm{GSNO}]}{K_{\mathrm{GSNO}} + [\mathrm{GSNO}]}$		
178	"GOR"	$\mathrm{GSSG + H^+ + NADPH \xrightarrow{Gor} 2\ GSH + NADP^+}$	$k_1 = 267\ s^{-1}$ $k_2 = 6.55\times10^5\ M^{-1}s^{-1}$ $K_{NADPH} = 2.2\times10^{-5}$ M $K_{GSSG} = 9.7\times10^{-5}$ M $K_1 = 0.022$ $K_2 = 3.9\times10^3\ M^{-1}$	(17) (18) (17) (17) (18) (18)
		$r = \frac{k_1[\mathrm{Gor}][\mathrm{GSSG}][\mathrm{NADPH}] + k_2[\mathrm{Gor}][\mathrm{GSSG}]^2[\mathrm{NADPH}]}{K_{\mathrm{NADPH}}[\mathrm{GSSG}] + K_{\mathrm{GSSG}}[\mathrm{NADPH}] + [\mathrm{GSSG}][\mathrm{NADPH}] + K_1[\mathrm{GSSG}]^2 + K_2[\mathrm{GSSG}]^2[\mathrm{NADPH}]}$		

179	"TRXR"	$Trx_{ox} + NADPH + H^+ \xrightarrow{TrxR} Trx_{red} + NADP^+$	k_{cat} = 41.25 s^{-1} K_{NADPH} = 4.6×10^{-6} M K_{Trxox} = 1.7×10^{-6} M	(19) (19) (19)
		$r = \frac{k_{cat}[TrxR][Trx_{ox}][NADPH]}{[Trx_{ox}][NADPH] + K_{NADPH}[Trx_{ox}] + K_{Trx_{ox}}[NADPH]}$		
180	"TRX_GSNO"	$Trx_{red} + GSNO \rightarrow Trx_{ox} + HNO + GSH$	k_{cat} = 0.02 s^{-1} K_{GSNO} = 1.0×10^{-5} M	(20) (20)
		$r = \frac{k_{cat}[Trx_{red}][GSNO]}{K_{GSNO} + [GSNO]}$		
181	"EX_O2air"	$O_{2,air} \rightleftharpoons O_{2,culture}$	$k_L a_{O2}$ = 1.25×10^{-3} s^{-1}	*b*
		$r = k_L a_{O_2}([O_2]_{sat} - [O_2])$		
182	"CYTbo_resp"	$O_2 + 2\ Q_8H_2 \xrightarrow{Cyo} 2\ H_2O + 2\ Q_8$	k_{cat} = 18.3–150 s^{-1} * $K_{iq1}K_{mq2}$ = 2.13 × 10^{-10} M^2 K_{Q8H2} = 5.3 × 10^{-5} M K_{O2} = 6.05 × 10^{-6} M	(21-23) (4,24) (25) (22)
		$r = \frac{k_{cat}[Cyo][O_2][Q_8H_2]^2}{K_{iq1}K_{mq2}[O_2] + K_{Q_8H_2}[Q_8H_2][O_2] + K_{O_2}[Q_8H_2]^2 + [Q_8H_2]^2[O_2]}$		
183	"CYTbd_resp"	$O_2 + 2\ Q_8H_2 \xrightarrow{Cyd} 2\ H_2O + 2\ Q_8$	k_{cat} = 12–469 s^{-1} * $K_{iq1}K_{mq2}$ = 2.13 × 10^{-10} M^2 K_{Q8H2} = 4.2 × 10^{-5} M K_{O2} = 2.7 × 10^{-7} M	(21,22,24) (24) (24) (22)
		$r = \frac{k_{cat}[Cyd][O_2][Q_8H_2]^2}{K_{iq1}K_{mq2}[O_2] + K_{Q_8H_2}[Q_8H_2][O_2] + K_{O_2}[Q_8H_2]^2 + [Q_8H_2]^2[O_2]}$		
184	"CYTbo_NO"	$Cyo + NO\bullet \rightleftharpoons Cyo(NO)$	$k_{on,NO\bullet}$ = (3.4–13.6)×10^6 M^{-1}s^{-1} * $k_{off,NO\bullet}$ = 0.03 s^{-1} K_{O2} = (6.05–60.5)×10^{-7} M *	(22) (22) (22)
		$r = \frac{k_{on,NO\bullet}[NO\bullet][Cyo]}{1 + \frac{[O_2]}{K_{O_2}}} - k_{off,NO\bullet}[Cyo(NO)]$		
185	"CYTbd_NO"	$Cyd + NO\bullet \rightleftharpoons Cyd(NO)$	$k_{on,NO\bullet}$ = (1.9–7.6)×10^8 M^{-1}s^{-1} * $k_{off,NO\bullet}$ = 0.163 s^{-1} K_{O2} = (2.7–27)×10^{-8} M *	(22) (22) (22)
		$r = \frac{k_{on,NO\bullet}[NO\bullet][Cyd]}{1 + \frac{[O_2]}{K_{O_2}}} - k_{off,NO\bullet}[Cyd(NO)]$		

186	"NDH1"	$NADH + Q_8 + H^+ \xrightarrow{NDH-1} NAD^+ + Q_8H_2$	k_{cat} = 50–600 s^{-1} * K_{NADH} = 7.2 × 10^{-6} M $K_{d,Q8}$ = 3.0 × 10^{-5} M $K_{m,Q8}$ = 3.0 × 10^{-5} M	(26,27) [h] (26) (4,28) (28)
		$r = \left(\frac{[P_{2Fe2S}(holo)]+[P_{4Fe4S}(holo)]}{[P_{FeS,TOT}]}\right)\left(\frac{k_{cat}[NDH1][Q_8][NADH]}{K_{NADH}K_{d,Q_8}+K_{NADH}[Q_8]+K_{m,Q_8}[NADH]+[Q_8][NADH]}\right)$ where: $[P_{FeS,TOT}]=[P_{2Fe2S}(holo)]+[P_{4Fe4S}(holo)]+[P_{2Fe2S}(DNIC)_2]+[P_{4Fe4S}(RRE)_2]+[P_{2Fe2S}(apo)]+[P_{4Fe4S}(apo)]$		
187	"NDH2"	$NADH + Q_8 + H^+ \xrightarrow{NDH-2} NAD^+ + Q_8H_2$	k_{cat} = 17.1–474 s^{-1} * K_{NADH} = 5.7 × 10^{-5} M $K_{d,Q8}$ = 5.9 × 10^{-6} M $K_{m,Q8}$ = 5.9 × 10^{-6} M	(4,29,30) (29) (4,31) (31)
		$r = \left(\frac{k_{cat}[NDH2][Q_8][NADH]}{K_{NADH}K_{d,Q_8}+K_{NADH}[Q_8]+K_{m,Q_8}[NADH]+[Q_8][NADH]}\right)$		
188	"NORVred"	$NorV_{ox} + NADH \rightarrow NorV_{red} + NAD^+ + H^+$	k_{cat} = 5.5×10^6 $M^{-1}s^{-1}$ $K_{i,NO\bullet}$ = 1.35×10^{-5} M	(32) (33)
		$r = \frac{k_{cat}[NorV_{ox}][NADH]}{1+\frac{[NO\bullet]}{K_{i,NO\bullet}}}$		
189	"NORVno"	$NorV_{red} + 2\ NO\bullet + 2\ H^+ \rightarrow NorV_{ox} + N_2O + H_2O$	k_{cat} = 7.45 s^{-1} $K_{NO\bullet}$ = (1–10)×10^{-7} M *	(34) (35,36)
		$r = \frac{k_{cat}[NorV_{red}][NO\bullet]}{K_{NO\bullet}+[NO\bullet]}$		
190	"NRFAno"	$NO\bullet + 6\ H^+ + 2.5\ NADH \xrightarrow{NrfA} NH_4^+ + H_2O + 2.5\ NAD^+ + 2.5\ H^+$	k_{cat} = 390 s^{-1} $K_{NO\bullet}$ = 3.0×10^{-4} M	(37) (38)
		$r = \frac{k_{cat}[NrfA][NO\bullet]}{K_{NO\bullet}+[NO\bullet]}$		
191	"HMP_transcr"	$\rightarrow mRNA_{hmp}$	k_{basal} = (0–2.78)×10^{-12} M·s^{-1} * k_{max} = (1.19–4.57)×10^{-10} M·s^{-1} * $K_{NO\bullet}$ = (1–1000)×10^{-8} M *	(39-41) [c] (39-41) (42,43) [d]
		$r = k_{basal} + (k_{max} - k_{basal})\frac{[NO\bullet]}{K_{NO\bullet}+[NO\bullet]}$		

192	"NORV_transcr"	→ $mRNA_{norV}$	k_{basal} = (0–2.78)×10^{-12} M·s^{-1} * k_{max} = (1.19–4.57)×10^{-10} M·s^{-1} * $K_{NO\bullet}$ = (1–1000)×10^{-8} M *	(39-41) (39-41) (42,43) [d]
	$r = k_{basal} + (k_{max} - k_{basal}) \frac{[NO\bullet]}{K_{NO\bullet} + [NO\bullet]}$			
193	"NRFA_transcr"	→ $mRNA_{nrfA}$	k_{max} = (1.19–4.57)×10^{-10} M·s^{-1} * K_{NO2-} = (1–1000)×10^{-6} M * K_{O2} = (1–100) ×10^{-12} M *	(39-41) *e* *e*
	$r = \frac{k_{max} K_{O_2} [NO_2^-]}{K_{NO_2^-} K_{O_2} + K_{O_2} [NO_2^-] + K_{NO_2^-} [O_2] + [NO_2^-][O_2]}$			
194	"HMP_translate"	→ $Hmp_{FAD,Fe3}$	$k_{Hmp\text{-}translate}$ = 0.057–1.49 s^{-1} * $k_{act,O2}$ = 0–10 * K_{O2} = 0–2.10×10^{-4} M *	(44-47) *f* (48) [g]
	$r = k_{Hmp\text{-}translate} [mRNA_{hmp}] \left(1 + \frac{k_{act,O_2} [O_2]}{K_{O_2} + [O_2]}\right)$			
195	"NORV_translate"	→ $NorV_{ox}$	$k_{NorV\text{-}translate}$ = 0.057–1.49 s^{-1} * $k_{act,O2}$ = 0–10 * K_{O2} = 0–2.10×10^{-4} M *	(44-47) *f* (48) [g]
	$r = k_{NorV\text{-}translate} [mRNA_{norV}] \left(1 + \frac{k_{act,O_2} [O_2]}{K_{O_2} + [O_2]}\right)$			
196	"NRFA_translate"	→ NrfA	$k_{NrfA\text{-}translate}$ = 0.057–1.49 s^{-1} * $k_{act,O2}$ = 0–10 * K_{O2} = 0–2.10×10^{-4} M *	(44-47) *f* (48) [g]
	$r = k_{NrfA\text{-}translate} [mRNA_{nrfA}] \left(1 + \frac{k_{act,O_2} [O_2]}{K_{O_2} + [O_2]}\right)$			

a. For additional details on model reactions, rate expressions, and parameters, see ref (3) regarding the original model construction.

b. The O_2 mass transfer coefficient ($k_L a_{O2}$) was measured in our experimental system (see *Supporting Methods* for additional details). This reaction takes place in "all" compartments (intracellular and extracellular).

c. The *hmp* basal transcription rate was restricted to ≤ 10 nM/h (2.78 × 10^{-12} M/s, approximately 100-fold less than the max. transcription rate), given the scarce levels of Hmp in untreated cells (49).

d. The NO• dissociation constant associated with activation of *hmp* and *norV* transcription was allowed to vary within the physiological range reported for NO• (nM to low μM).

e. The constant governing NO_2^- regulation of *nrfA* transcription was varied in the μM range, whereas the constant governing O_2-mediated inhibition of transcription was assumed to be orders of magnitude lower given the anaerobic dependence of *nrfA* expression (50,51).

f. Assumed a maximum O_2-mediated influence on translation of approximately one order of magnitude.

g. O_2 constant associated with translation activation was permitted to vary from zero to air-saturated O_2 concentration at 37°C (210 μM) (48).

h. Enzyme function was assumed to be affected by [Fe-S] damage. See ref (4) for additional details.

Table S2. AIC of optimal parameter sets for each optimization stage. The Akaike information criterion (AIC) calculated (see *Methods*, Main text) for the best-fit parameter set of each optimization stage is presented along with the corresponding number of optimized parameters (equivalent to $k - 1$ in Equations 6 and 7, Main text), number of data points (n), and sum of the squared residuals (SSR) between the measured and simulated [NO•] curves.

Stage	**SSR**	**Optimized parameters**	**Data points**	**AIC**
1	33.76	17	1076	−3688
2	29.19	136	1076	−3567
3	15.45	19	1076	−4525
4	10.48	23	1076	−4935

Table S3. Growth time at different O_2 concentrations. "Growth time" was quantified as the time required for a WT *E. coli* culture to grow from an initial OD_{600} of 0.01 to an OD_{600} of 0.20 in 20 mL of MOPS + 10 mM glucose in a 250 mL baffled shake flask at 37°C and 200 rpm. Times are listed as the mean ± SEM for at least 3 independent experiments. The O_2 concentration corresponds to the concentration of dissolved O_2 in cell-free media that was in equilibrium with that particular environment.

[O_2] (μM)	**Growth time (h)**
0	7.31 ± 0.08
5	5.60 ± 0.01
10	5.27 ± 0.05
20	5.02 ± 0.01
50	5.07 ± 0.05

Table S4. Reaction deletion analysis of [NO•] oscillation dynamics. Shown is the minimal set of model reactions (name, description, and stoichiometric equation) necessary to (*A*) maintain sufficient quality-of-fit (ER < 10) relative to the full model, or (*B*) maintain [NO•] oscillations, for 50 μM DPTA treatment of WT culture at 5 μM O_2.

(*A*) Minimal set of reactions necessary to maintain quality-of-fit (ER < 10).

Reaction name	**Deletion eliminates oscillations***	**Reaction description**	**Reaction equation**
EX_NOautox	False	NO• autoxidation	$2\ NO\bullet + O_2 \rightarrow 2\ NO_2\bullet$
EX_NO_NO2r	False	NO• reaction with NO_2•	$NO\bullet + NO_2\bullet \rightarrow N_2O_3$
HMP1/2[†]	True	Hmp reduction	$Hmp(FAD\text{-}Fe^{3+}) + NAD(P)H + H^+ \rightarrow Hmp(FADH_2\text{-}Fe^{3+}) + NAD(P)^+$
HMP3	True	Hmp electron transfer	$Hmp(FADH_2\text{-}Fe^{3+}) \rightarrow Hmp(FADH\bullet\text{-}Fe^{2+}) + H^+$
HMP4	True	Hmp O_2 binding	$Hmp(FADH\bullet\text{-}Fe^{2+}) + O_2 \rightarrow Hmp(FADH\bullet\text{-}Fe^{2+})\text{-}O_2$
HMP6	True	Hmp-O_2 oxygenation of NO•	$Hmp(FADH\bullet\text{-}Fe^{2+})\text{-}O_2 + NO\bullet \rightarrow Hmp(FADH\bullet\text{-}Fe^{3+})\text{-}ONOO^-$
HMP7	True	NO_3^- release from Hmp	$Hmp(FADH\bullet\text{-}Fe^{3+})\text{-}ONOO^- \rightarrow Hmp(FADH\bullet\text{-}Fe^{3+}) + NO_3^-$
HMP8	True	Hmp electron transfer	$Hmp(FADH\bullet\text{-}Fe^{3+}) \rightarrow Hmp(FAD\text{-}Fe^{2+}) + H^+$
HMP9	False	Hmp O_2 binding	$Hmp(FAD\text{-}Fe^{2+}) + O_2 \rightarrow Hmp(FAD\text{-}Fe^{2+})\text{-}O_2$
HMP11	True	Hmp-O_2 oxygenation of NO•	$Hmp(FAD\text{-}Fe^{2+})\text{-}O_2 + NO\bullet \rightarrow Hmp(FAD\text{-}Fe^{3+})\text{-}ONOO^-$
HMP12	True	NO_3^- release from Hmp	$Hmp(FAD\text{-}Fe^{3+})\text{-}ONOO^- \rightarrow Hmp(FAD\text{-}Fe^{3+}) + NO_3^-$
HMP13	False	Hmp NO• binding	$Hmp(FADH\bullet\text{-}Fe^{2+}) + NO\bullet \rightarrow Hmp(FADH\bullet\text{-}Fe^{2+})\text{-}NO$
HMP15	True	Hmp NO• reduction	$Hmp(FADH\bullet\text{-}Fe^{2+})\text{-}NO \rightarrow Hmp(FADH\bullet\text{-}Fe^{3+}) + NO^-$
HMP16	False	Hmp NO• binding	$Hmp(FAD\text{-}Fe^{2+}) + NO\bullet \rightarrow Hmp(FAD\text{-}Fe^{2+})\text{-}NO$
HMP18	True	Hmp NO• reduction	$Hmp(FAD\text{-}Fe^{2+})\text{-}NO \rightarrow Hmp(FAD\text{-}Fe^{3+}) + NO^-$
HMP20	False	Hmp reduction	$Hmp(FAD\text{-}Fe^{2+}) + NADPH + H^+ \rightarrow Hmp(FADH_2\text{-}Fe^{2+}) + NADP^+$
HMP21	False	Hmp NO• binding	$Hmp(FADH_2\text{-}Fe^{2+}) + NO\bullet \rightarrow Hmp(FADH_2\text{-}Fe^{2+})\text{-}NO$
HMP23	True	Hmp NO• reduction	$Hmp(FADH_2\text{-}Fe^{2+})\text{-}NO \rightarrow Hmp(FADH_2\text{-}Fe^{3+}) + NO^-$
HMP24	True	Hmp O_2 binding	$Hmp(FADH_2\text{-}Fe^{2+}) + O_2 \rightarrow Hmp(FADH_2\text{-}Fe^{2+})\text{-}O_2$
HMP28	True	Hmp-O_2 oxygenation of NO•	$Hmp(FADH_2\text{-}Fe^{2+})\text{-}O_2 + NO\bullet \rightarrow Hmp(FADH_2\text{-}Fe^{3+})\text{-}ONOO^-$
HMP29	True	NO_3^- release from Hmp	$Hmp(FADH_2\text{-}Fe^{3+})\text{-}ONOO^- \rightarrow Hmp(FADH\bullet\text{-}Fe^{2+}) + NO_3^- + H^+$
EX_NOdonor	True	NONOate dissociation	$NONOate \rightarrow 2\ NO\bullet$
EX_NOout	True	NO• loss to gas phase	$NO\bullet \rightarrow gas$
hmpFe2h_deg	False	Hmp degradation	$Hmp(FADH\bullet\text{-}Fe^{2+}) \rightarrow$
hmpFe2h2_deg	False	Hmp degradation	$Hmp(FADH_2\text{-}Fe^{2+}) \rightarrow$
hmpFe2h_o2_deg	False	Hmp degradation	$Hmp(FADH\bullet\text{-}Fe^{2+})\text{-}O_2 \rightarrow O_2$
hmpFe2h2_o2_deg	False	Hmp degradation	$Hmp(FADH_2\text{-}Fe^{2+})\text{-}O_2 \rightarrow O_2$

hmpFe2_no_deg	False	Hmp degradation	$Hmp(FAD\text{-}Fe^{2+})\text{-}NO \rightarrow NO\bullet$
hmpFe2h_no_deg	False	Hmp degradation	$Hmp(FADH\bullet\text{-}Fe^{2+})\text{-}NO \rightarrow NO\bullet$
hmpFe2h2_no_deg	False	Hmp degradation	$Hmp(FADH_2\text{-}Fe^{2+})\text{-}NO \rightarrow NO\bullet$
norVred_o2	True‡	O_2-mediated NorV inactivation	$NorV_{red} + O_2 \rightarrow$
CYTbo_NO	True	Cytochrome *bo* NO• binding	$NO\bullet + Cyt\textit{bo} \leftrightarrow Cyt\textit{bo}\text{-}NO$
CYTbd_NO	True	Cytochrome *bd* NO• binding	$NO\bullet + Cyt\textit{bd} \leftrightarrow Cyt\textit{bd}\text{-}NO$
NORVred	False	NorV reduction	$NorV_{ox} + NADH \rightarrow NorV_{red} + NAD^+ + H^+$
NORVno	False	NorV NO• reduction	$NorV_{red} + 2\ NO\bullet + 2\ H^+ \rightarrow NorV_{ox} + N_2O + H_2O$
EX_O2gas	True	O_2 transfer with gas phase	$O_{2,gas} \leftrightarrow O_2$
HMP_translate	True	Hmp translation	$\rightarrow Hmp(FAD\text{-}Fe^{3+})$
NORV_translate	False	NorV translation	$\rightarrow NorV_{ox}$
CYTbo_resp	False	Cytochrome *bo* O_2 reduction	$O_2 + 2\ Q_8H_2 \rightarrow 2\ H_2O + 2\ Q_8$
CYTbd_resp	True	Cytochrome *bd* O_2 reduction	$O_2 + 2\ Q_8H_2 \rightarrow 2\ H_2O + 2\ Q_8$
NDH1	True	NADH dehydrogenase I quinone reduction	$NADH + Q_8 + H^+ \rightarrow NAD^+ + Q_8H_2$
HMP_transcr	True	*hmp* transcription	$\rightarrow mRNA_{\textit{hmp}}$
RNA_hmp_deg	True	$mRNA_{\textit{hmp}}$ degradation	$mRNA_{\textit{hmp}} \rightarrow$
NORV_transcr	False	*norV* transcription	$\rightarrow mRNA_{\textit{norV}}$
RNA_norV_deg	True‡	$mRNA_{\textit{norV}}$ degradation	$mRNA_{\textit{norV}} \rightarrow$
All Hmp reactions	True	(all reactions associated with Hmp)	--
All CYT reactions	True	(all reactions associated with Cyt *bo* & *bd*)	--
All NorV reactions	False	(all reactions associated with NorV)	--

* Reactions from this minimal set were deleted individually (or in groups of all Hmp-, CYT-, and NorV-related reactions), and the resulting simulated [NO•] curve (at 5 μM O_2) was visually inspected to determine whether oscillations were eliminated ("True") or remained ("False").

† A second minimal set of reactions was identified, and was identical as the set presented here, except HMP1 was substituted for HMP2, where the reaction involved a reduction of Hmp by NADPH instead of NADH.

‡ Two NorV-related reactions eliminated oscillations when deleted individually ("norVred_o2" and "RNA_norV_deg"), but had no effect on oscillations when deleted simultaneously with all other NorV-related reactions.

(*B*) Minimal set of reactions necessary to maintain [NO•] oscillations.

Reaction name	**Reaction description**	**Reaction equation**
HMP1/2[†]	Hmp reduction	$Hmp(FAD\text{-}Fe^{3+}) + NAD(P)H + H^+ \rightarrow Hmp(FADH_2\text{-}Fe^{3+}) + NAD(P)^+$
HMP3	Hmp electron transfer	$Hmp(FADH_2\text{-}Fe^{3+}) \rightarrow Hmp(FADH\bullet\text{-}Fe^{2+}) + H^+$
HMP4	Hmp O_2 binding	$Hmp(FADH\bullet\text{-}Fe^{2+}) + O_2 \rightarrow Hmp(FADH\bullet\text{-}Fe^{2+})\text{-}O_2$
HMP6	Hmp-O_2 oxygenation of NO•	$Hmp(FADH\bullet\text{-}Fe^{2+})\text{-}O_2 + NO\bullet \rightarrow Hmp(FADH\bullet\text{-}Fe^{3+})\text{-}ONOO^-$
HMP7	NO_3^- release from Hmp	$Hmp(FADH\bullet\text{-}Fe^{3+})\text{-}ONOO^- \rightarrow Hmp(FADH\bullet\text{-}Fe^{3+}) + NO_3^-$
HMP8	Hmp electron transfer	$Hmp(FADH\bullet\text{-}Fe^{3+}) \rightarrow Hmp(FAD\text{-}Fe^{2+}) + H^+$
HMP11	Hmp-O_2 oxygenation of NO•	$Hmp(FAD\text{-}Fe^{2+})\text{-}O_2 + NO\bullet \rightarrow Hmp(FAD\text{-}Fe^{3+})\text{-}ONOO^-$
HMP12	NO_3^- release from Hmp	$Hmp(FAD\text{-}Fe^{3+})\text{-}ONOO^- \rightarrow Hmp(FAD\text{-}Fe^{3+}) + NO_3^-$
HMP15	Hmp NO• reduction	$Hmp(FADH\bullet\text{-}Fe^{2+})\text{-}NO \rightarrow Hmp(FADH\bullet\text{-}Fe^{3+}) + NO^-$
HMP18	Hmp NO• reduction	$Hmp(FAD\text{-}Fe^{2+})\text{-}NO \rightarrow Hmp(FAD\text{-}Fe^{3+}) + NO^-$
HMP23	Hmp NO• reduction	$Hmp(FADH_2\text{-}Fe^{2+})\text{-}NO \rightarrow Hmp(FADH_2\text{-}Fe^{3+}) + NO^-$
HMP24	Hmp O_2 binding	$Hmp(FADH_2\text{-}Fe^{2+}) + O_2 \rightarrow Hmp(FADH_2\text{-}Fe^{2+})\text{-}O_2$
HMP28	Hmp-O_2 oxygenation of NO•	$Hmp(FADH_2\text{-}Fe^{2+})\text{-}O_2 + NO\bullet \rightarrow Hmp(FADH_2\text{-}Fe^{3+})\text{-}ONOO^-$
HMP29	NO_3^- release from Hmp	$Hmp(FADH_2\text{-}Fe^{3+})\text{-}ONOO^- \rightarrow Hmp(FADH\bullet\text{-}Fe^{2+}) + NO_3^- + H^+$
EX_NOdonor	NONOate dissociation	$NONOate \rightarrow 2\ NO\bullet$
EX_NOout	NO• loss to gas phase	$NO\bullet \rightarrow gas$
CYTbo_NO	Cytochrome *bo* NO• binding	$NO\bullet + Cyt\textit{bo} \leftrightarrow Cyt\textit{bo}\text{-}NO$
CYTbd_NO	Cytochrome *bd* NO• binding	$NO\bullet + Cyt\textit{bd} \leftrightarrow Cyt\textit{bd}\text{-}NO$
EX_O2gas	O_2 transfer with gas phase	$O_{2,gas} \leftrightarrow O_2$
HMP_translate	Hmp translation	$\rightarrow Hmp(FAD\text{-}Fe^{3+})$
CYTbd_resp	Cytochrome *bd* O_2 reduction	$O_2 + 2\ Q_8H_2 \rightarrow 2\ H_2O + 2\ Q_8$
NDH1	NADH dehydrogenase I quinone reduction	$NADH + Q_8 + H^+ \rightarrow NAD^+ + Q_8H_2$
HMP_transcr	*hmp* transcription	$\rightarrow mRNA_{hmp}$
RNA_hmp_deg	$mRNA_{hmp}$ degradation	$mRNA_{hmp} \rightarrow$

[†] A second minimal set of reactions was identified, and was identical as the set presented here, except HMP1 was substituted for HMP2, where the reaction involved a reduction of Hmp by NADPH instead of NADH.

Table S5. Primers used for cPCR confirmation of genetic deletions. Each deletion was confirmed with colony PCR (cPCR) using two primer sets: (1) a forward and reverse primer within the coding sequence of the deleted gene, and (2) a forward primer upstream of the deleted gene and a reverse primer within the kan^R coding sequence (for mutations with kan^R cassette in place of the gene), or a forward and reverse primer upstream and downstream (respectively) of the deleted gene (for mutations from which kan^R had been cured).

Primer sequence (5′ → 3′)	**Gene**	**Description**
CCGAATCATTGTGCGATAACA	*hmp*	Forward primer, upstream of the *hmp* gene
GCAAAATCGGTGACGGTAAA		Reverse primer, downstream of the *hmp* gene
TCCCTTTACTGGTGGAAACG		Forward primer, within the *hmp* gene
CACGCCCAGATCCACTAACT		Reverse primer, within the *hmp* gene
CCAGCACATCAACGGAAAAA	*norV*	Forward primer, upstream of the *norV* gene
GACTGGGAAGTGCGTGATTT		Forward primer, within the *norV* gene
CGGAAGCGTAAACCAGTCAT		Reverse primer, within the *norV* gene
TTTCTCATCACCCAGTTGTCACTCTAA	*cyoA*	Forward primer, upstream of the *cyoA* gene
GAGGTCAGCCACTCTTTCCA		Reverse primer, downstream of the *cyoA* gene
ATGAGACTCAGGAAATACAATAAAAGTTTG		Forward primer, within the *cyoA* gene
GTCCATGCCTTCCATACCTTC		Reverse primer, within the *cyoA* gene
ATGCAGAAATATGCCCGTCT	*appB*	Forward primer, upstream of the *appB* gene
GTGTCAGCCAACCCAGTTTT		Reverse primer, downstream of the *appB* gene
GATGATGAACGCCGGATAGT		Forward primer, within the *appB* gene
TACGGCGGAGAGTTTCTGTT		Reverse primer, within the *appB* gene
TGGCTTCCTGCTTCTGGCAA	*cydB*	Forward primer, upstream of the *cydB* gene
TCTGCTGATTGGTTTTGCAG		Forward primer, within the *cydB* gene
CATACGTGCAGTCAGGATGG		Reverse primer, within the *cydB* gene
ATGATGGATACTTTCTCGGCAGGAG	kan^R	Reverse primer, within the kan^R gene

Table S6. Training of respiratory module. Parameters involved in O_2 respiration were trained on [O_2] measurements of exponential-phase WT *E. coli* cultures growing in an environment of 50 μM O_2 (SI Appendix, Supporting Methods and Fig. S14*B*). Values were permitted to vary within bounds (min and max), for which reference(s) are provided. Optimal values were the parameter set yielding the minimum SSR.

#	Parameter	Parameter description/reaction involved	Min.	Max.	Units	Ref.	Optimal
1	$k_{Cyo,cat}$	Cytochrome *bo* terminal oxidase; k_{cat}	18.3	150	s^{-1}	(21-23)	125
2	$k_{Cyd,cat}$	Cytochrome *bd* terminal oxidase; k_{cat}	12	469	s^{-1}	(21,22,24)	460
3	$k_{NDH1,cat}$	NADH dehydrogenase I; k_{cat}	50	600	s^{-1}	(26,27)	498
4	$k_{NDH2,cat}$	NADH dehydrogenase II; k_{cat}	17.1	474	s^{-1}	(29,30)	438
5	$[Cyo]_0$	Initial concentration of cytochrome *bo*	1.58×10^{-8}	1.58×10^{-6}	M	(52) [a]	1.33×10^{-6}
6	$[Cyd]_0$	Initial concentration of cytochrome *bd*	1.06×10^{-8}	1.06×10^{-6}	M	(52) [a]	1.04×10^{-6}
7	$[Q_8]_0$	Initial concentration of ubiquinone-8	4.48×10^{-5}	4.48×10^{-3}	M	(53) [a,b]	3.71×10^{-3}
8	$[Q_8H_2]_0$	Initial concentration of ubiquinol-8	4.48×10^{-5}	4.48×10^{-3}	M	(53) [a,b]	2.72×10^{-4}
9	$[NDH1]_0$	Initial concentration of NADH dehydrogenase I	2.70×10^{-8}	2.70×10^{-6}	M	(47) [a]	2.21×10^{-6}
10	$[NDH2]_0$	Initial concentration of NADH dehydrogenase II	3.05×10^{-9}	3.05×10^{-7}	M	(54) [a]	1.19×10^{-7}

a. The concentration of biomolecules were permitted to vary within an order of magnitude of the reported value. Concentrations were converted from molecules/cell to molar assuming a cell volume of 3.2×10^{-15} L (55).

b. ubiquinone and ubiquinol concentrations were converted from μmol/g dry cell weight (53) to molar assuming cell density of 448 gDW/L (47).

SUPPORTING REFERENCES

1. Adolfsen KJ, Brynildsen MP (2015) A Kinetic Platform to Determine the Fate of Hydrogen Peroxide in *Escherichia coli*. *PLoS Comput Biol* 11(11):e1004562.
2. Zamora-Sillero E, Hafner M, Ibig A, Stelling J, Wagner A (2011) Efficient characterization of high-dimensional parameter spaces for systems biology. *BMC Syst Biol* 5:142.
3. Robinson JL, Brynildsen MP (2013) A Kinetic Platform to Determine the Fate of Nitric Oxide in *Escherichia coli*. *PLoS Comput Biol* 9(5):e1003049.
4. Robinson JL, Miller RV, Brynildsen MP (2014) Model-driven identification of dosing regimens that maximize the antimicrobial activity of nitric oxide. *Metab Eng Commun* 1:12-18.
5. Urbina HD, Silberg JJ, Hoff KG, Vickery LE (2001) Transfer of sulfur from IscS to IscU during Fe/S cluster assembly. *J Biol Chem* 276(48):44521-44526.
6. Prischi F, *et al.* (2010) Structural bases for the interaction of frataxin with the central components of iron-sulphur cluster assembly. *Nat Commun* 1:95.
7. Bonomi F, Iametti S, Ta D, Vickery LE (2005) Multiple turnover transfer of [2Fe2S] clusters by the iron-sulfur cluster assembly scaffold proteins IscU and IscA. *J Biol Chem* 280(33):29513-29518.
8. Terato H, *et al.* (2002) Novel repair activities of AlkA (3-methyladenine DNA glycosylase II) and endonuclease VIII for xanthine and oxanine, guanine lesions induced by nitric oxide and nitrous acid. *Nucleic Acids Res* 30(22):4975-4984.
9. Zhao B, O'Brien PJ (2011) Kinetic mechanism for the excision of hypoxanthine by *Escherichia coli* AlkA and evidence for binding to DNA ends. *Biochemistry* 50(20):4350-4359.
10. Wong I, Lundquist AJ, Bernards AS, Mosbaugh DW (2002) Presteady-state analysis of a single catalytic turnover by *Escherichia coli* uracil-DNA glycosylase reveals a "pinch-pull-push" mechanism. *J Biol Chem* 277(22):19424-19432.
11. Stivers JT, Pankiewicz KW, Watanabe KA (1999) Kinetic mechanism of damage site recognition and uracil flipping by *Escherichia coli* uracil DNA glycosylase. *Biochemistry* 38(3):952-963.
12. Faure V, Saparbaev M, Dumy P, Constant JF (2005) Action of multiple base excision repair enzymes on the 2'-deoxyribonolactone. *Biochem Biophys Res Commun* 328(4):1188-1195.
13. McClure WR, Jovin TM (1975) The steady state kinetic parameters and non-processivity of *Escherichia coli* deoxyribonucleic acid polymerase I. *J Biol Chem* 250(11):4073-4080.
14. Bertram JG, Oertell K, Petruska J, Goodman MF (2010) DNA polymerase fidelity: comparing direct competition of right and wrong dNTP substrates with steady state and pre-steady state kinetics. *Biochemistry* 49(1):20-28.
15. Lehman IR (1974) DNA ligase: structure, mechanism, and function. *Science* 186(4166):790-797.
16. Liu L, *et al.* (2001) A metabolic enzyme for S-nitrosothiol conserved from bacteria to humans. *Nature* 410(6827):490-494.
17. Scrutton NS, Deonarain MP, Berry A, Perham RN (1992) Cooperativity Induced by a Single Mutation at the Subunit Interface of a Dimeric Enzyme - Glutathione-Reductase. *Science* 258(5085):1140-1143.

18. Carlberg I, Mannervik B (1975) Purification and characterization of the flavoenzyme glutathione reductase from rat liver. *J Biol Chem* 250(14):5475-5480.
19. Mulrooney SB (1997) Application of a single-plasmid vector for mutagenesis and high-level expression of thioredoxin reductase and its use to examine flavin cofactor incorporation. *Protein Expres Purif* 9(3):372-378.
20. Sengupta R, *et al.* (2007) Thioredoxin catalyzes the denitrosation of low-molecular mass and protein S-nitrosothiols. *Biochemistry* 46(28):8472-8483.
21. Rice CW, Hempfling WP (1978) Oxygen-limited continuous culture and respiratory energy conservation in *Escherichia coli*. *J Bacteriol* 134(1):115-124.
22. Mason MG, *et al.* (2009) Cytochrome bd confers nitric oxide resistance to *Escherichia coli*. *Nat Chem Biol* 5(2):94-96.
23. Bolgiano B, Salmon I, Poole RK (1993) Reactions of the membrane-bound cytochrome bo terminal oxidase of *Escherichia coli* with carbon monoxide and oxygen. *Biochim Biophys Acta* 1141(1):95-104.
24. Junemann S, Butterworth PJ, Wrigglesworth JM (1995) A suggested mechanism for the catalytic cycle of cytochrome bd terminal oxidase based on kinetic analysis. *Biochemistry* 34(45):14861-14867.
25. Yap LL, *et al.* (2010) The quinone-binding sites of the cytochrome bo3 ubiquinol oxidase from *Escherichia coli*. *Biochim Biophys Acta* 1797(12):1924-1932.
26. Verkhovskaya ML, Belevich N, Euro L, Wikstrom M, Verkhovsky MI (2008) Real-time electron transfer in respiratory complex I. *Proc Natl Acad Sci U S A* 105(10):3763-3767.
27. Leif H, Sled VD, Ohnishi T, Weiss H, Friedrich T (1995) Isolation and characterization of the proton-translocating NADH: ubiquinone oxidoreductase from *Escherichia coli*. *Eur J Biochem* 230(2):538-548.
28. David P, Baumann M, Wikstrom M, Finel M (2002) Interaction of purified NDH-1 from *Escherichia coli* with ubiquinone analogues. *Biochim Biophys Acta* 1553(3):268-278.
29. Jaworowski A, Campbell HD, Poulis MI, Young IG (1981) Genetic identification and purification of the respiratory NADH dehydrogenase of *Escherichia coli*. *Biochemistry* 20(7):2041-2047.
30. Villegas JM, Volentini SI, Rintoul MR, Rapisarda VA (2011) Amphipathic C-terminal region of *Escherichia coli* NADH dehydrogenase-2 mediates membrane localization. *Arch Biochem Biophys* 505(2):155-159.
31. Bjorklof K, Zickermann V, Finel M (2000) Purification of the 45 kDa, membrane bound NADH dehydrogenase of *Escherichia coli* (NDH-2) and analysis of its interaction with ubiquinone analogues. *FEBS Lett* 467(1):105-110.
32. Vicente JB, *et al.* (2007) Kinetics of electron transfer from NADH to the *Escherichia coli* nitric oxide reductase flavorubredoxin. *FEBS J* 274(3):677-686.
33. Girsch P, deVries S (1997) Purification and initial kinetic and spectroscopic characterization of NO reductase from *Paracoccus denitrificans*. *Biochim Biophys Acta* 1318(1-2):202-216.
34. Gomes CM, *et al.* (2002) A novel type of nitric-oxide reductase. *Escherichia coli* flavorubredoxin. *J Biol Chem* 277(28):25273-25276.
35. Gardner AM, Helmick RA, Gardner PR (2002) Flavorubredoxin, an inducible catalyst for nitric oxide reduction and detoxification in *Escherichia coli*. *J Biol Chem* 277(10):8172-8177.

36. Vicente JB, *et al.* (2008) Kinetic characterization of the *Escherichia coli* nitric oxide reductase flavorubredoxin. *Methods Enzymol* 437:47-62.
37. Poock SR, Leach ER, Moir JW, Cole JA, Richardson DJ (2002) Respiratory detoxification of nitric oxide by the cytochrome c nitrite reductase of *Escherichia coli*. *J Biol Chem* 277(26):23664-23669.
38. van Wonderen JH, Burlat B, Richardson DJ, Cheesman MR, Butt JN (2008) The nitric oxide reductase activity of cytochrome c nitrite reductase from *Escherichia coli*. *J Biol Chem* 283(15):9587-9594.
39. Kennell D, Riezman H (1977) Transcription and translation initiation frequencies of the *Escherichia coli lac* operon. *J Mol Biol* 114(1):1-21.
40. Liang S, *et al.* (1999) Activities of constitutive promoters in *Escherichia coli*. *J Mol Biol* 292(1):19-37.
41. So LH, *et al.* (2011) General properties of transcriptional time series in *Escherichia coli*. *Nat Genet* 43(6):554-560.
42. Allen BW, Liu J, Piantadosi CA (2005) Electrochemical detection of nitric oxide in biological fluids. *Methods Enzymol* 396:68-77.
43. Wang C, Trudel LJ, Wogan GN, Deen WM (2003) Thresholds of nitric oxide-mediated toxicity in human lymphoblastoid cells. *Chem Res Toxicol* 16(8):1004-1013.
44. Bieling P, Beringer M, Adio S, Rodnina MV (2006) Peptide bond formation does not involve acid-base catalysis by ribosomal residues. *Nat Struct Mol Biol* 13(5):423-428.
45. Johansson M, Bouakaz E, Lovmar M, Ehrenberg M (2008) The kinetics of ribosomal peptidyl transfer revisited. *Mol Cell* 30(5):589-598.
46. Liang ST, Xu YC, Dennis P, Bremer H (2000) mRNA composition and control of bacterial gene expression. *J Bacteriol* 182(11):3037-3044.
47. Sundararaj S, *et al.* (2004) The CyberCell Database (CCDB): a comprehensive, self-updating, relational database to coordinate and facilitate in silico modeling of *Escherichia coli*. *Nucleic Acids Res* 32(Database issue):D293-295.
48. Montgomery HAC, Thom NS, Cockburn A (1964) Determination of dissolved oxygen by the winkler method and the solubility of oxygen in pure water and sea water. *J Appl Chem* 14(7):280-296.
49. Poole RK, *et al.* (1996) Nitric oxide, nitrite, and Fnr regulation of *hmp* (flavohemoglobin) gene expression in *Escherichia coli* K-12. *J Bacteriol* 178(18):5487-5492.
50. Browning DF, Lee DJ, Spiro S, Busby SJ (2010) Down-regulation of the *Escherichia coli* K-12 *nrf* promoter by binding of the NsrR nitric oxide-sensing transcription repressor to an upstream site. *J Bacteriol* 192(14):3824-3828.
51. Spiro S (2006) Nitric oxide-sensing mechanisms in *Escherichia coli*. *Biochem Soc Trans* 34(Pt 1):200-202.
52. Cotter PA, Chepuri V, Gennis RB, Gunsalus RP (1990) Cytochrome *o* (*cyoABCDE*) and *d* (*cydAB*) Oxidase Gene Expression in *Escherichia coli* Is Regulated by Oxygen, pH, and the *fnr* Gene Product. *J Bacteriol* 172(11):6333-6338.
53. Bekker M, *et al.* (2007) Changes in the redox state and composition of the quinone pool of *Escherichia coli* during aerobic batch-culture growth. *Microbiology* 153(Pt 6):1974-1980.
54. Taniguchi Y, *et al.* (2010) Quantifying *E. coli* proteome and transcriptome with single-molecule sensitivity in single cells. *Science* 329(5991):533-538.

55. Volkmer B, Heinemann M (2011) Condition-dependent cell volume and concentration of *Escherichia coli* to facilitate data conversion for systems biology modeling. *PLoS One* 6(7):e23126.